

# Glioblastoma: does the pre-treatment geometry matter? A postcontrast T1 MRI-based study

Julián Pérez-Beteta<sup>1</sup> · Alicia Martínez-González<sup>1</sup> · David Molina<sup>1</sup> · Mariano Amo-Salas<sup>1</sup> · Belén Luque<sup>1</sup> · Elena Arregui<sup>2</sup> · Manuel Calvo<sup>2</sup> · José M. Borrás<sup>2</sup> · Carlos López<sup>2</sup> · Marta Claramonte<sup>2</sup> · Juan A. Barcia<sup>3</sup> · Lidia Iglesias<sup>3</sup> · Josué Avecillas<sup>3</sup> · David Albillo<sup>4</sup> · Miguel Navarro<sup>4</sup> · José M. Villanueva<sup>4</sup> · Juan C. Paniagua<sup>4</sup> · Juan Martino<sup>5</sup> · Carlos Velásquez<sup>5</sup> · Beatriz Asenjo<sup>6</sup> · Manuel Benavides<sup>6</sup> · Ismael Herruzo<sup>6</sup> · María del Carmen Delgado<sup>7</sup> · Ana del Valle<sup>7</sup> · Anthony Falkov<sup>8</sup> · Philippe Schucht<sup>9</sup> · Estanislao Arana<sup>10</sup> · Luis Pérez-Romasanta<sup>4</sup> · Víctor M. Pérez-García<sup>1</sup>

Received: 29 March 2016 / Revised: 11 May 2016 / Accepted: 25 May 2016 / Published online: 21 June 2016  
© European Society of Radiology 2016

## Abstract

**Background** The potential of a tumour's volumetric measures obtained from pretreatment MRI sequences of glioblastoma (GBM) patients as predictors of clinical outcome has been controversial. Mathematical models of GBM growth have suggested a relation between a tumour's geometry and its aggressiveness.

**Methods** A multicenter retrospective clinical study was designed to study volumetric and geometrical measures on pretreatment postcontrast T1 MRIs of 117 GBM patients.

Clinical variables were collected, tumours segmented, and measures computed including: contrast enhancing (CE), necrotic, and total volumes; maximal tumour diameter; equivalent spherical CE width and several geometric measures of the CE "rim". The significance of the measures was studied using proportional hazards analysis and Kaplan-Meier curves.

**Results** Kaplan-Meier and univariate Cox survival analysis showed that total volume [ $p=0.034$ , Hazard ratio (HR)=1.574], CE volume ( $p=0.017$ , HR=1.659), spherical rim width ( $p=0.007$ , HR=1.749), and geometric heterogeneity ( $p=0.015$ , HR=1.646) were significant parameters in terms of overall survival (OS). Multivariable Cox analysis for OS provided the later two parameters as age-adjusted predictors of OS ( $p=0.043$ , HR=1.536 and  $p=0.032$ , HR=1.570, respectively).

**Conclusion** Patients with tumours having small geometric heterogeneity and/or spherical rim widths had significantly better prognosis. These novel imaging biomarkers have a strong individual and combined prognostic value for GBM patients.

## Key Points

- Three-dimensional segmentation on magnetic resonance images allows the study of geometric measures.
- Patients with small width of contrast enhancing areas have better prognosis.
- The irregularity of contrast enhancing areas predicts survival in glioblastoma patients.

✉ Julián Pérez-Beteta  
Julian.Perez@uclm.es

<sup>1</sup> Laboratory of Mathematical Oncology, Edificio Politécnico, Instituto de Matemática Aplicada a la Ciencia y la Ingeniería, Universidad de Castilla-La Mancha, Avenida de Camilo José Cela, 3, 13071 Ciudad Real, Spain

<sup>2</sup> Hospital General de Ciudad Real, c/ Obispo Rafael Torija, Ciudad Real, Spain

<sup>3</sup> Hospital Clínico San Carlos, Madrid, Spain

<sup>4</sup> Hospital Universitario de Salamanca, Salamanca, Spain

<sup>5</sup> Hospital Marqués de Valdecilla, Santander, Spain

<sup>6</sup> Hospital Carlos Haya, Málaga, Spain

<sup>7</sup> Facultad de Matemáticas, Universidad de Sevilla, Sevilla, Spain

<sup>8</sup> Auckland Radiation Oncology, Auckland, New Zealand

<sup>9</sup> Neurosurgery Department, Bern Inselspital, Bern, Switzerland

<sup>10</sup> Instituto Valenciano de Oncología, Valencia, Spain

**Keywords** Glioblastoma · Predictors of survival · GBM geometry · Contrast enhancement · Mathematical model

## Abbreviations

|              |  |
|--------------|--|
| GBM          | Glioblastoma   |
| PFS          | Progression-free Survival                              |
| OS           | Overall survival                                       |
| KPS          | Karnofsky performance status                           |
| VAK          | Volume-Age-KPS   |
| 3D           | Three-dimensional                                      |
| CE           | Contrast enhancing                                     |
| DICOM        | Digital imaging and communication in medicine          |
| $V_{CE}$     | CE volume  |
| $V_I$        | Inner volume   |
| V            | Total postcontrast T1 tumour volume                    |
| $d_{max}$ 3D | Maximum tumour diameter in 3D                          |
| $\delta_s$   | Average size of CE rim                                 |
| $G_H$        | Measure of geometric heterogeneity of the CE rim width |
| HR           | Hazard ratio   |
| 2D           | Bidimensional  |
| Gd           | Gadolinium   |
| $p$          | $p$ -value   |

## Introduction

Glioblastoma (GBM) is the most frequent malignant primary brain tumour and the most lethal type, with a median survival of 14.6 months for those patients receiving the standard of care, i.e. maximal safe surgery plus radiotherapy and chemotherapy [1]. MRI is routinely used for diagnosis, treatment planning, response evaluation, and follow-up.

Typical GBM appearance upon diagnosis on MRI consists of an enhancing ring mass with central non-enhancing core of necrosis observed mainly on contrast enhanced T1-weighted images; this is surrounded by an area of signal hyperintensity on fluid-attenuated inversion recovery (FLAIR) or T2 images representing oedema that is well known to contain infiltrated tumour cells.

Recently there has been an increased use of advanced imaging techniques to characterize the connection of the so-called radiophenotype with the tumour genotype (see e.g. recent reviews for GBM [2, 3]). However, the use of those techniques requires further research and validation to achieve broad clinical applicability. Thus, contrast enhanced T1 and T2/FLAIR are still the gold standard for diagnosis and treatment planning [4].

Some works have studied geometrical measures measured on pretreatment T1 and FLAIR images as prognostic “biomarkers”. Specifically, Iliadis et al. [5] analyzed volumetric data of 50 GBM patients to confirm the importance of age and performance status in progression-free survival (PFS) and overall survival (OS) of patients, while volume was not significant. Mazurowski et al. [6] showed the association of survival in 68 GBM patients with the proportion of enhancing

tumour and major axis length. Zinn et al. [7] used tumour volume, patient age, and Karnofsky performance status (KPS), to develop a simple 3-point scoring system, the Volume-Age-KPS (VAK) classification, classifying patients into groups with significant survival differences. Other studies have added sets of imaging descriptors to the usual age and KPS to improve the predictive power of survival models for GBM patients with modest results [8] or combined several imaging features using data mining of imaging variables [9].

Pérez-García et al. [10] developed a mathematical model predicting a positive correlation between the spherical rim width and the tumour’s biological aggressiveness, which would have an impact on overall survival.

Our purpose in this study was to study the prognostic potential of full three-dimensional geometrical measures of postcontrast T1 MRIs in a large set of GBM patients with high-resolution images in the absence of previous treatment.

## Patients and methods

**Patients** A retrospective study including patients from six medical institutions was organized. The respective ethical committees approved the study. Patients with pathologically confirmed diagnosis of GBM diagnosed in the period 2006–2014 were included in the study. The inclusion criteria were availability of the relevant clinical variables and availability of pretreatment postcontrast T1 MRI. Multifocal GBMs without contrast enhancement (CE) and very diffuse tumours with no clear boundaries were excluded from the study. A total of 117 patients complied with inclusion criteria. Patients’ characteristics are summarized in Table 1.

The extent of resection was determined from the postcontrast T1 MRI usually within 48 h after surgery. Gross total resection was defined as the absence of visible CE.

PFS and OS were assessed. Recurrence-free patients at last follow-up were considered censored events for the PFS analysis. Overall survival was measured from time of surgery to death. Patients who were still alive at last follow-up were considered censored events for the OS analysis.

**Image acquisition parameters** Two different field strengths were used to obtain the MRIs of this retrospective study: 1.5 Tesla (100 patients) and 3 Tesla (17 patients). MRIs were of high spatial resolution as shown in Table 1. As to the other acquisition parameters, they satisfy the recent consensus recommendations for standardized brain tumour imaging [11].

**Image analysis** The pretreatment postcontrast T1 MRI Digital Imaging and Communication in Medicine (DICOM) files were imported into the scientific software package Matlab (R2015b, The MathWorks, Inc., Natick, MA, USA) and pre-processed using a semi-automatic image segmentation

**Table 1** Summary of patient characteristics, MRI data, and volumetric parameters for the 117 patients included in the study

| Median or Mean value (range or percentage) |  |
|--|--|
| Patient characteristics:                   |  |
| Median age, years (Range)                  | 62 (31 – 85)   |
| Sex (Percentage)                           | 60 Male (51.28 %); 57 Female (48.72 %)   |
| Median survival (Range)                    | 363 days (17 – 1794)   |
| Type of resection (Percentage)             | 62 Total resection (52.99 %)<br>32 Subtotal resection (27.35 %)<br>23 Biopsy (19.66 %) |
| First-line treatment received (Percentage) | 16 No treatment (13.68 %)<br>2 RT (1.71 %)<br>7 TMZ (5.98 %)<br>92 RT+TMZ (78.63 %)    |
| MRI characteristics:                       |  |
| Average pixel spacing (Range)              | 0.88 mm (0.46 – 1.02)  |
| Average spacing between slices (Range)     | 1.07 mm (0.70 – 2.00)  |
| Average slice thickness (Range)            | 1.62 mm (1.00 – 2.00)  |
| Average slices per patient (Range)         | 170 mm (80 – 248)  |
| Field strength (Percentage)                | 1.5 Tesla for 100 patients (85.47 %)<br>3 Tesla for 17 patients (14.53 %)              |
| Relevant volumetric parameters             |  |
| Average tumour volume (Range)              | 32.68 cm <sup>3</sup> (0.66–132.54)  |
| Average contrast enhancing volume (Range)  | 17.69 cm <sup>3</sup> (0.20 – 86.33)   |
| Average maximal tumour diameter (Range)    | 5.05 cm (1.37– 11.09)  |
| Average spherical rim width (Range)        | 0.47 cm (0.10 – 1.05)  |

procedure considering two possible regions: the enhancing tumour and the inner tumour region. Then, tumour segmentations were manually corrected slice by slice. Figure 1 summarizes the segmentation process.

**Geometrical measures** After the segmentation, a set of geometrical 3D measures were computed automatically. First, we calculated volumetric measures on the reconstructed tumours: the CE volume ( $V_{CE}$ ), the volume surrounded by the CE areas or inner volume ( $V_I$ ), and the total postcontrast T1 tumour volume ( $V = V_{CE} + V_I$ ). In most cases the inner volume corresponds to necrotic areas. Also, the maximum tumour diameter in 3D ( $d_{max}$  3D) and some measures of the tumour surface irregularity were computed.

The average size for the CE rim was called spherical rim width ( $\delta_s$ ) because it can be obtained from a spherical approximation from the total and CE volume, using the formula.

$$\delta_s = \sqrt[3]{\frac{3}{4\pi}(\sqrt[3]{V} - \sqrt[3]{V_I})} \approx 0.62(\sqrt[3]{V} - \sqrt[3]{V_I})$$

In order to characterize the CE rim structure we constructed the surfaces enclosing the CE areas (inner and outer). For every point on these surfaces the minimal distance to the other surface

was computed, providing a large set of distances that was used to construct histograms of rim sizes. This histogram was characterized by many measures (median, mean, positions of the quartiles, etc.). Of them, the most relevant found was the geometric heterogeneity of the CE rim width ( $G_H$ ). This is defined as the difference between the values of quartiles 3 and 4 of the distribution of CE rim widths divided by quartile 4, i.e..

$$G_H = \frac{(\delta_4 - \delta_3)}{\delta_4}$$

The geometric heterogeneity uses the difference between the values of quartiles 3 and 4, i.e. the size of the region of the most asymmetric distances of the tumour, divided by the longest rim width in the tumour. This is a normalized measure of the tumour's asymmetry with values in the range [0,1]. Figure 4 provides visual examples of the meaning of the most relevant geometrical parameters.

**Statistical methods** To identify parameters associated with prognosis we used Kaplan-Meier curves and log-rank analysis. Kaplan-Meier curves measure the fraction of patients living for a certain amount of time [12]. An important advantage of this method is that it can take into account some types of

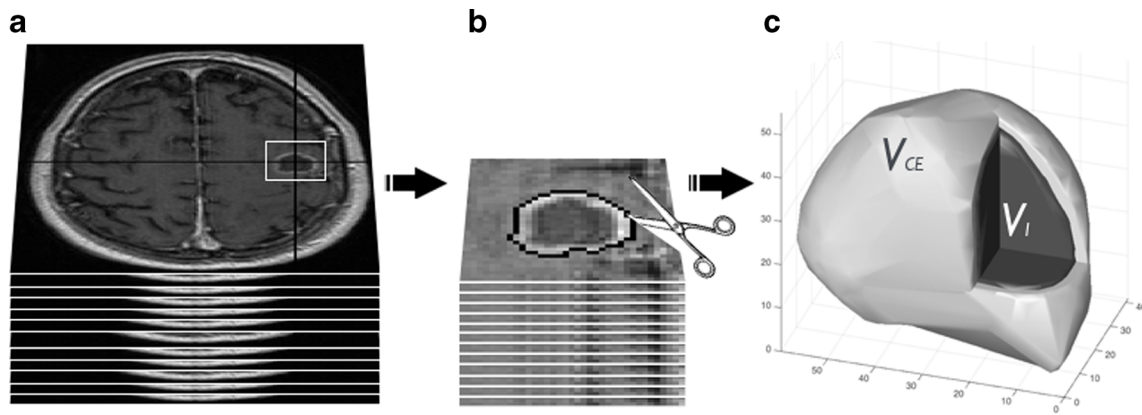


**Fig. 1** Image segmentation procedure: tumours described by the MRI slices (a) were semi-automatically segmented and then manually corrected by an image expert. The resulting segmented slices (b) are then joined to construct a full 3D tumour (c)

censored data, particularly if a patient withdraws from a study, is lost to follow-up, or is alive without event occurrence at last follow-up. It can be calculated for two groups of subjects, showing their statistical difference in the survival. A 2-tailed significance level ( $p$ -value) of  $p < 0.05$  was used.

We searched for robust thresholds separating patient populations in subgroups with significant differences in terms of OS and PFS. To find the optimal thresholds, we computed the  $p$ -values for the full range of thresholds of each geometrical variable with subgroups of at least 30 patients and looked for the minimum  $p$ -value. Only minima located in low- $p$  regions of the parameter space were considered in order to discard purely statistical fluctuations.

We also computed the hazard ratio (HR) as indicator of risk by using a single-variable Cox proportional hazards regression analysis.

We also computed the correlations between the significant variables of the previous analysis. Normality of the variables was analyzed using Kolmogorov-Smirnov test. Because of the results of the normality analysis, Spearman's correlation coefficient was chosen to study the relation between independent quantitative variables.

We used multivariate proportional hazard Cox analysis with a stepwise method in order to construct a predictive model. To guarantee the robustness of the geometric significant variables, we performed two different types of analysis for both the OS and the PFS. The first one including all the significant geometrical variables and the second one also including the age in order to evaluate its effect in the multivariable model. SPSS software (v. 22.0.00) was used for the statistical analysis.

## Results

### Overall survival

The best thresholds for the total volume, CE volume, geometric heterogeneity and spherical rim width were  $15.6 \text{ cm}^3$

( $p = 0.034$ ),  $10 \text{ cm}^3$  ( $p = 0.017$ ),  $0.6146$  ( $p = 0.015$ ), and  $4.4 \text{ mm}$  ( $p = 0.007$ ), respectively (see Table 3). The increases in the median survival times for the favourable subgroups were 133 days ( $V < 15.6 \text{ cm}^3$ ), 199 days ( $V_{CE} < 10 \text{ cm}^3$ ), 155 days ( $G_H < 0.6146$ ), and 213 days ( $\delta_s < 4.4 \text{ mm}$ ). Figure 2 shows the Kaplan-Meier survival curves for each of those significant variables.

### Progression free survival

The geometric heterogeneity ( $p = 0.012$ ) was statistically significant in terms of progression-free survival. However, the total volume ( $p = 0.093$ ), the CE volume ( $p = 0.075$ ), and the spherical rim width ( $p = 0.077$ ) were only marginal predictors of PFS.

### Spherical rim width ( $\delta_s$ )

The threshold for the most significant parameter, the spherical rim width ( $\delta_s$ ), was found to be  $4.4 \text{ mm}$ . Interestingly, a broad range of threshold values ranging from  $3.7 \text{ mm}$  to  $5.1 \text{ mm}$  were found to provide significant results ( $p < 0.05$ ). Within this interval, patient subgroups ranged from 37 (below threshold) and 80 (above threshold) patients to 75 (below threshold) and 42 (above threshold) patients. Thus,  $\delta_s$  was not only the most significant geometrical variable for OS but also the most robust one.

### Geometric heterogeneity of the rim width ( $G_H$ )

The only other significant geometrical measure according to the Kaplan-Meier analysis for both OS and PFS was the geometric heterogeneity ( $G_H$ ). The threshold value found was  $0.6146$  and the groups were well balanced with 68 and 49 patients, respectively. The median OS in both subgroups were 509 days (patients with  $G_H < 0.6146$ ) and 354 days ( $G_H > 0.6146$ ). Results for PFS were 351 ( $G_H < 0.6146$ ) and 229 ( $G_H > 0.6146$ ) days, respectively.

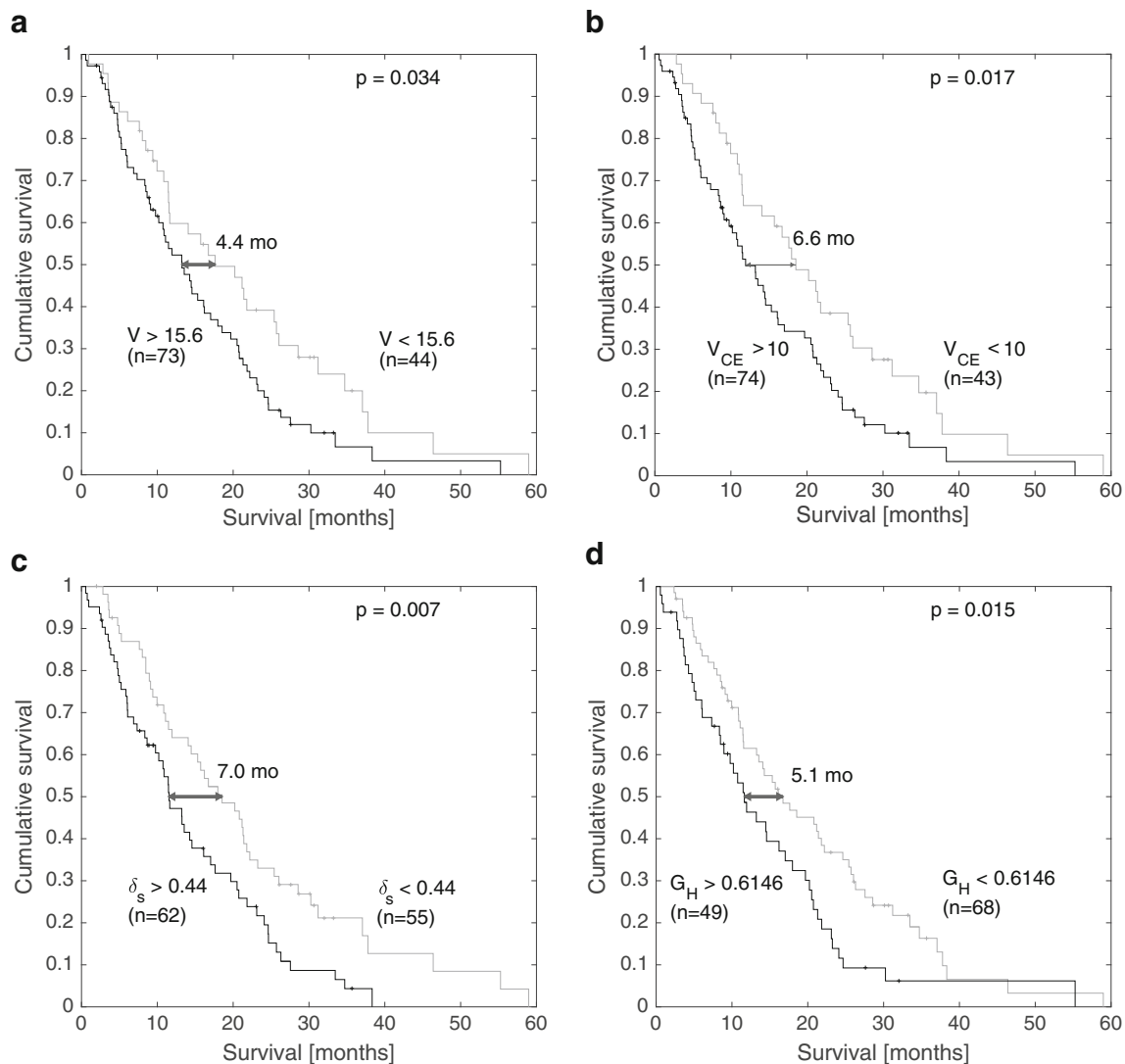


**Fig. 2** Kaplan-Meier curves for the significant geometrical variables for OS. The median difference, the  $p$ -value, and the number of patients in each subgroup are shown for: **a** the total volume  $V$ , **b** the CE volume  $V_{CE}$ , **c** the spherical rim width  $\delta_s$ , and **d** the geometric heterogeneity  $G_H$

### Classification in terms of prognosis

We classified patients in terms of prognosis by considering three groups: double positive (+,+) = ( $\delta_s$  and  $G_H$  above the threshold), double negative (-,-) = ( $\delta_s$  and  $G_H$  below the threshold), and single positive (+,-) = ( $\delta_s$  above and  $G_H$  below or vice versa). We found significant OS differences between the first two groups (Fig. 3,  $p < 0.001$ ). The double positive group of patients had the worse prognosis. There were no long-term double positive survivors while 40 % of double negative patients lived for more than 24 months. In general, single positive patients (whatever of both imaging biomarkers was positive) had better prognosis than double positive patients and worse than double negative patients (Fig. 3). Figure 4 shows four different tumour geometries in terms of the four previous groups.

### Correlations and multivariable cox analysis

We computed the Spearman's correlation coefficient between every pair of variables and the associated  $p$ -values. The geometric heterogeneity ( $G_H$ ), spherical rim width ( $\delta_s$ ), and age, all significant in the Kaplan-Meier analysis (Table 2), are mutually uncorrelated. The volumetric variables ( $V_{CE}$ ,  $V_I$ ,  $V$ ,  $d_{max}$  3D) were strongly correlated.

The results of the multivariable Cox analysis are summarized in Table 3. We first performed an analysis including all the significant geometrical variables of Table 2. For OS, the geometric heterogeneity ( $G_H$ ) and the spherical rim width ( $\delta_s$ ) were significant in terms of survival. The hazard ratios were 1.588 ( $G_H$ ) and 1.696 ( $\delta_s$ ). For PFS, the only variable remaining significant in the multivariable model was the geometric heterogeneity (HR = 1.672).



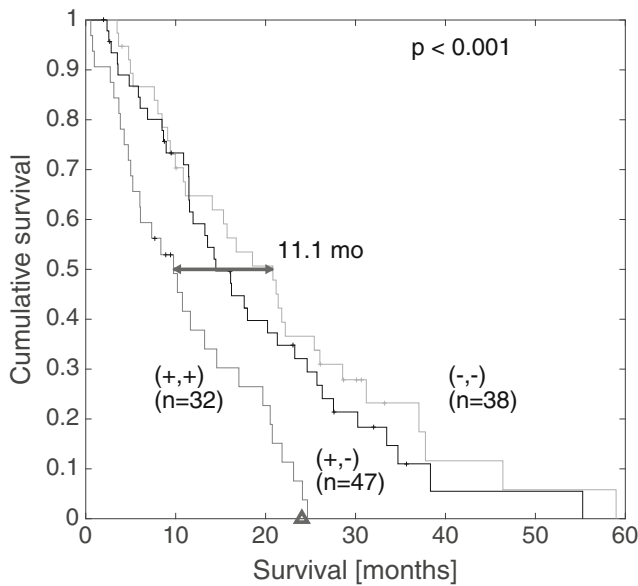


**Fig. 3** Kaplan-Meier curves for the significant variables spherical rim width ( $\delta_s$ ) and geometric heterogeneity ( $G_H$ ) considering three different groups: double positive patients (+,+)= $\delta_s$  and  $G_H$  above the threshold), double negative (-,-)= $\delta_s$  and  $G_H$  below the threshold), and single positive (+,-)=(whatever imaging biomarker  $\delta_s^+$  or  $G_H^+$  is positive). The median difference and  $p$ -value correspond to the comparison between the (+,+) and the (-,-) curves

As a second step, we performed the same multivariable analysis using age as adjusting factor. Interestingly, only the same two geometrical variables were significant for both the OS and the PFS analysis. For OS, the hazard ratios were 1.036, 1.570, and 1.536 for age, geometric heterogeneity ( $G_H$ ), and spherical rim width ( $\delta_s$ ), respectively.

**Discussion**

Previous studies have identified MRI-derived variables to be associated with survival. Some of the more relevant ones are the ratio of T2-FLAIR image signal to T1 image tumour volume [13], the volume of enhancing tumour crossing the corpus callosum [14], the CE tumour volume [9, 14], the proportion of enhancing tumour [6], and the longest axis length of tumour [6, 15].

However, to our knowledge, most previous analyses have been either qualitative, or when quantitative the analysis has been two-dimensional. Moreover, most studies have been carried out using limited resolution images. No study has tried to characterize fully the complex 3D nature of irregular rim-shaped CE areas present in GBMs. The need for that kind of 3D study using high-resolution data to obtain reliable conclusions has been put forward recently [11]. A very recent study

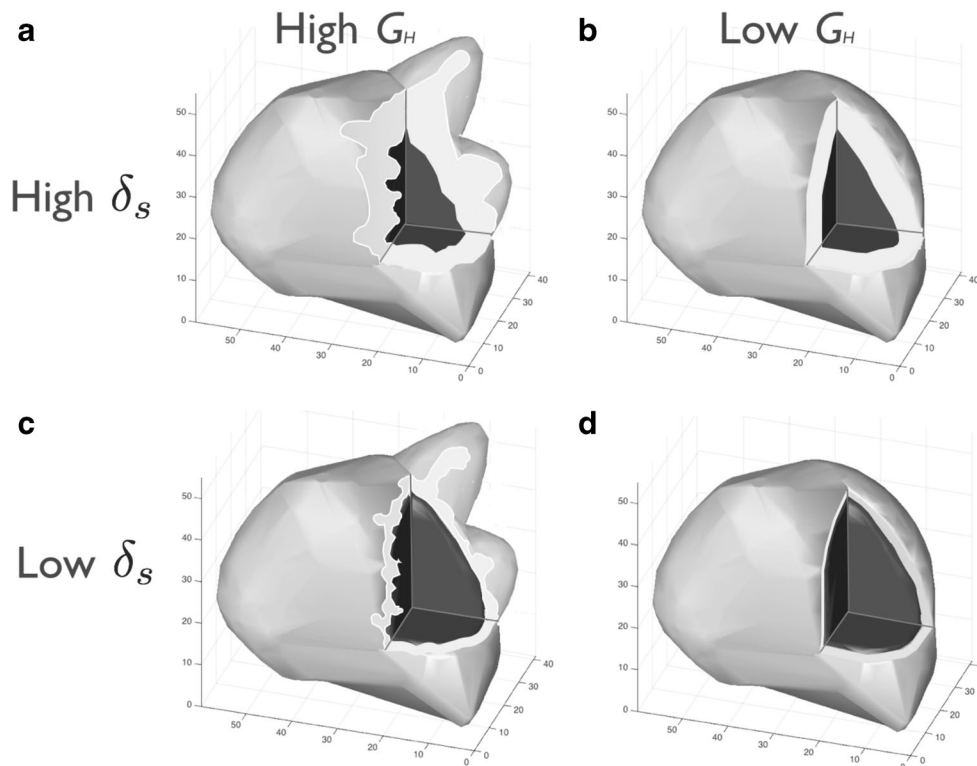


**Fig. 4** Four different tumour geometries in terms of the  $\delta_s$  and  $G_H$  possible configurations: **a** corresponds to a tumour characterized by high spherical rim width and high geometric heterogeneity (bad prognosis), **b** shows a tumour characterized by high spherical rim width

and low geometric heterogeneity, **c** corresponds to a tumour characterized by low spherical rim width and high geometric heterogeneity, and **d** shows a tumour characterized by low spherical rim width and low geometric heterogeneity (good prognosis)

**Table 2** Summary of univariate Cox and Kaplan-Meier analysis for the more representative variables included in the study

| Variables                                 | Overall Survival      |                  | Progression-Free Survival |                 |
|---|-----------------------|------------------|---------------------------|-----------------|
|   | HR, (CI-95 %)         | <i>p</i> -value  | HR, (CI-95 %)             | <i>p</i> -value |
| Age (years)                               | 1.040 (1.019, 1.062)  | <b>&lt;0.000</b> | 1.037 (1.016, 1.058)      | <b>0.001</b>    |
| Age (<64 vs. >64)                         | 2.048 (1.361, 3.080)  | <b>&lt;0.001</b> | 1.821 (1.215, 2.731)      | <b>0.003</b>    |
| Mean: Age (<61.5 vs. >61.5)               | 1.833 (1.224, 2.744)  | <b>0.003</b>     | 1.543 (1.031, 2.308)      | <b>0.033</b>    |
| Median: Age (<62 vs. >62)                 | 1.829 (1.223, 2.735)  | <b>0.003</b>     | 1.541 (1.031, 2.303)      | <b>0.033</b>    |
| Necrotic volume ( $V_f$ , $cm^3$ )        | 1.001 (0.989, 1.014)  | 0.817            | 0.999 (0.987, 1.012)      | 0.914           |
| $V_f$ (<7.55 vs. >7.55)                   | 1.452 (0.962, 2.192)  | 0.074            | 1.392 (0.923, 2.100)      | 0.112           |
| Mean: $V_f$ (<15.0 vs. >15.0)             | 1.243 (0.809, 1.912)  | 0.319            | 1.133 (0.741, 1.733)      | 0.563           |
| Median: $V_f$ (<9.44 vs. >9.44)           | 1.366 (0.913, 2.044)  | 0.128            | 1.328 (0.887, 1.987)      | 0.166           |
| Total volume ( $V$ , $cm^3$ )             | 1.003 (0.996-1.010)   | 0.368            | 1.002 (0.995, 1.008)      | 0.645           |
| $V$ (<15.6 vs. >15.6)                     | 1.574 (1.032, 2.400)  | <b>0.034</b>     | 1.429 (0.940, 2.173)      | 0.093           |
| Mean: $V$ (<32.68 vs. >32.68)             | 1.212 (0.793, 1.854)  | 0.374            | 1.184 (0.778, 1.803)      | 0.430           |
| Median: $V$ (<26.3883 vs. >26.3883)       | 1.124 (0.753, 1.676)  | 0.567            | 1.066 (0.715, 1.589)      | 0.753           |
| CE volume ( $V_{CE}$ , $cm^3$ )           | 1.010 (0.997, 1.023)  | 0.129            | 1.006 (0.994, 1.019)      | 0.308           |
| $V_{CE}$ (<10.0 vs. >10.0)                | 1.659 (1.088, 2.529)  | <b>0.017</b>     | 1.459 (0.959, 2.218)      | 0.075           |
| Mean: $V_{CE}$ (<17.69 vs. >17.69)        | 1.316 (0.874, 1.981)  | 0.187            | 1.210 (0.808, 1.810)      | 0.354           |
| Median: $V_{CE}$ (<14.01 vs. >14.01)      | 1.358 (0.904, 2.040)  | 0.139            | 1.231 (0.825, 1.837)      | 0.307           |
| Spherical rim width ( $\delta_s$ , cm)    | 1.658 (0.566, 4.855)  | 0.356            | 1.210 (0.424, 3.453)      | 0.721           |
| $\delta_s$ (<0.44 vs. >0.44)              | 1.749 (1.160, 2.637)  | <b>0.007</b>     | 1.434 (0.959, 2.144)      | 0.077           |
| Mean: $\delta_s$ (<0.47 vs. >0.47)        | 1.678 (1.114, 2.527)  | <b>0.012</b>     | 1.460 (0.976, 2.185)      | 0.064           |
| Median: $\delta_s$ (<0.45 vs. >0.45)      | 1.442 (0.961, 2.165)  | 0.076            | 1.225 (0.821, 1.827)      | 0.318           |
| Maximum rim width ( $\delta_{max}$ , cm)  | 1.013 (0.562, 1.829)  | 0.965            | 0.902 (0.507, 1.603)      | 0.725           |
| $\delta_{max}$ (<0.88 vs. >0.88)          | 1.170 (0.776, 1.765)  | 0.452            | 1.151 (0.763, 1.737)      | 0.501           |
| Mean: $\delta_{max}$ (<0.99 vs. >0.99)    | 1.087 (0.722, 1.636)  | 0.690            | 0.961 (0.640, 1.443)      | 0.848           |
| Median: $\delta_{max}$ (<0.92 vs. >0.92)  | 1.177 (0.789, 1.757)  | 0.424            | 1.104 (0.739, 1.649)      | 0.629           |
| Mean rim width ( $\delta_{mean}$ , cm)    | 0.529 (0.087, 3.202)  | 0.488            | 0.372 (0.063, 2.195)      | 0.275           |
| $\delta_{mean}$ (<0.27 vs. >0.27)         | 1.238 (0.803, 1.908)  | 0.333            | 1.106 (0.717, 1.705)      | 0.648           |
| Mean: $\delta_{mean}$ (<0.32 vs. >0.32)   | 0.939 (0.616, 1.430)  | 0.769            | 0.889 (0.585, 1.351)      | 0.581           |
| Median: $\delta_{mean}$ (<0.31 vs. >0.32) | 1.014 (0.675, 1.525)  | 0.945            | 0.965 (0.644, 1.446)      | 0.862           |
| Maximum 3D diameter ( $d_{max}$ 3D, cm)   | 1.089 (0.967, 1.226)  | 0.160            | 1.074 (0.955, 1.208)      | 0.232           |
| $d_{max}$ 3D (<4.56 vs. >4.56)            | 1.427 (0.946, 2.153)  | 0.088            | 1.309 (0.870, 1.971)      | 0.195           |
| Mean: $d_{max}$ 3D (<5.04 vs. >5.04)      | 1.336 (0.893, 1.998)  | 0.157            | 1.325 (0.887, 1.979)      | 0.167           |
| Median: $d_{max}$ 3D (<4.89 vs. >4.89)    | 1.277 (0.853, 1.912)  | 0.234            | 1.227 (0.820, 1.836)      | 0.318           |
| Geometric heterogeneity ( $G_H$ )         | 2.342 (0.346, 15.872) | 0.383            | 2.782 (0.440, 17.596)     | 0.277           |
| $G_H$ (<0.6146 vs. >0.6146)               | 1.646 (1.096, 2.474)  | <b>0.015</b>     | 1.672 (1.114, 2.508)      | <b>0.012</b>    |
| Mean: $G_H$ (<0.5892 vs. >0.5892)         | 1.109 (0.736, 1.671)  | 0.620            | 1.188 (0.790, 1.787)      | 0.406           |
| Median: $G_H$ (<0.5933 vs. >0.5933)       | 1.347 (0.901, 2.014)  | 0.145            | 1.501 (1.000, 2.251)      | <b>0.048</b>    |

Significant *p*-values are boldfaced

has analyzed a series of imaging features on 3D images and has identified several significant ones including the volume, CE volume and major axis length [16].

In comparison to previous studies: (i) our dataset of 117 patients was larger than that of most previous studies (typically below 100). (ii) Only high-resolution MRIs were included, thus reducing noise due to large voxel size and/or voxel interspacing. (iii) We included only pretreatment images to

avoid post-therapy imaging artefacts/distortions. (iv) The analysis was fully 3D on the reconstructed tumours. In addition to the more “classical” volumetric measures of the different regions [17], we included the maximal 3D diameter (instead of the major axis), a measure of the tumour’s surface, and the full set of geometrical measures characterizing the geometry of the CE rim as described in the methods section.

**Table 3** Results of the multivariate Cox analysis

|                           | Overall Survival      |                 | Progression-Free Survival |                 |
|---------------------------|-----------------------|-----------------|---------------------------|-----------------|
|                           | HR (95 % CI)          | <i>p</i> -value | HR (95 % CI)              | <i>p</i> -value |
| Volumetric multivariate   |                       |                 |                           |                 |
| $G_H$                     | 1.588 (1.053 - 2.396) | 0.027           | 1.672 (1.114 - 2.508)     | 0.013           |
| $\delta_s$                | 1.696 (1.122 - 2.566) | 0.012           | -                         | -               |
| Age-adjusted multivariate |                       |                 |                           |                 |
| Age                       | 1.036 (1.015 - 1.058) | 0.001           | 1.036 (1.015 - 1.057)     | 0.001           |
| $G_H$                     | 1.570 (1.039 - 2.372) | 0.032           | 1.689 (1.125 - 2.536)     | 0.012           |
| $\delta_s$                | 1.536 (1.014 - 2.327) | 0.043           | -                         | -               |

Since our study was based on high resolution MRIs and our main interest was on the geometry of CE regions we considered only postcontrast preoperative T1 images. Some qualitative features of T2/FLAIR have been found in previous studies to have a limited prognostic value. However, those image modalities are not available in sufficient resolution to allow for an accurate 3D reconstruction of the tumour.

It has been hypothesized that the tumour surface may play a relevant role in tumour progression [18]. Up to the spatial resolution of our study, the irregularity of the tumour surface was neither a predictor of OS or PFS as evidenced by the non-significance of the corresponding geometric parameter.

The Kaplan-Meier analysis demonstrated that the total volume, CE volume, geometric heterogeneity, and spherical rim width were significant variables. Regarding volume, the threshold found was small (15.6 cm<sup>3</sup>), which means that small tumours have better prognosis, probably because a lower biological aggressiveness, reduced treatment side effects and much larger fraction of completely resected tumours (64 % vs. 46 % in our dataset).

It is remarkable that the simplest geometrical measure of the rim size, the spherical rim width ( $\delta_s$ ), was the outstanding parameter for the OS analysis, able to classify the patient population into two subgroups with the highest statistical significance ( $p=0.007$ ) and the largest difference between median survivals (213 days). It is very interesting that the computation of this novel prognostic indicator is very simple, since only volumetric measures of the CE and necrotic regions are required. As the threshold for this variable was very flexible, this measure is a powerful imaging biomarker predicting survival.

The differences in treatment between the two subgroups ( $\delta_s^+$  and  $\delta_s^-$ ) were smaller than in the case of the groups obtained from total volume (or diameter) as cutoff variables.  $\delta_s^-$  patients received complete resections in 58 % of the cases and 83 % of these patients received chemo-radiotherapy (Stupp regime).  $\delta_s^+$  patients' tumours were completely resected in 49 % cases and 73 % of these patients received chemo-radiotherapy. The differences in treatment between both subgroups cannot explain the

large differences observed between the median survivals. This points to essentially different biological behaviour between both subgroups (i.e. not only a “size” effect).

The mathematical model of Perez-Garcia et al. [10] allows computing the tumour's growth speed as a function of several biological parameters: the tumour cell's average infiltration speed, the proliferation rate, and the tumour cell loss factor rate. It turns out that the rim width has a similar dependence on the parameters as the tumour's growth speed. Thus, based on the mathematical model, one would expect tumours with large rims to grow faster than those with small rims. This would have direct implications on survival. Our results corroborate the predictions of the mathematical model.

The other significant geometrical variable was the geometric heterogeneity ( $G_H$ ). The threshold value found (0.6146) points to a bad prognosis of tumours with more than 60 % of the full range of possible width values occupied by the top 25 % of the measures. The median survival of  $G_H^-$ , low geometric heterogeneity patients, is 5 months longer than that of  $G_H^+$  patients. One may expect a tumour to present this kind of heterogeneity either because of the existence of underlying anatomical structures (i.e. fibre tracts) supporting growth and allowing infiltration in a specific direction or because of the presence of regions with more aggressive tumour cell phenotypes. The fact that the percentage of total resections is substantially smaller in the large  $G_H$  group (60 % vs. 43 %) supports that at least a fraction of those tumours grow along fibre tracts, making complete resection without functional loss less feasible. It may happen that these patients benefit from either more aggressive resections around finger areas or radiotherapy dose escalation whenever possible in order to target those potentially more harmful cells.

The geometric heterogeneity ( $G_H$ ) and spherical rim width ( $\delta_s$ ) parameters were identified by the multivariate Cox analysis as the most relevant geometrical variables (either age-adjusted or not), in line with the results from the Kaplan-Meier analysis. In fact, their combined use leads to the definition of a set of doubly negative patients ( $G_H^-$  and  $\delta_s^-$ ) with the longest median survival and doubly positive patients ( $G_H^+$  and  $\delta_s^+$ ) with almost 1 year less median survival. Moreover, there were almost no long-term survivors in the double positive group.

As a final comment, the main interest of the analysis developed in this paper is the definition of simple geometric quantities of direct prognostic significance. A prospective study design is needed to validate the utility of these imaging biomarkers. Several recent works have studied the potential of complex sets of bidimensional (2D) or aggregated 2D image-based features to predict molecular subtypes in GBM patients [18, 19]. Genomic data was not available for our patient set. However, it is interesting that several geometrical measures were powerful predictors of survival. Their combination, together with other relevant variables (e.g., age, KPS) might be



used to develop a classification of patients in terms of prognosis. The main advantage would be the simplicity of the approach in comparison with more complex sets of image features used to classify patients in some recent works [18, 19]. Because of their relevant prognostic value the geometric variables found to be significant in this study could also help to predict a benefit from surgery and other therapies.

## Conclusions

Our analysis of geometrical measures of postcontrast T1 pre-treatment images found the total volume, CE volume, spherical rim width, and geometric heterogeneity of the CE rim as individual predictors of overall survival for GBM patients. Of them spherical rim width and geometric heterogeneity were the two most significant ones. Small values of those variables led to an improved survival as predicted by previous mathematical models. Small spherical rim widths and/or low geometric heterogeneity were associated with improved survival on multivariate analysis and allowed to define three subgroups: double positive, double negative, and mixed with different outcomes.

Thus, the two novel measures of the tumour's CE rim in T1+Gd MRI images have a strong individual and combined prognostic value, reflecting different biological behaviour between the subgroups.

**Acknowledgments** We would like to acknowledge Juan Belmonte (Universidad de Castilla-La Mancha) for discussions. The scientific guarantor of this publication is Víctor M. Manuel Pérez-García (Victor.PerezGarcia@uclm.es), full professor and head of Department of Mathematics at Universidad de Castilla-La Mancha (Spain). The authors of this manuscript declare no relationships with any companies, whose products or services may be related to the subject matter of the article. This work has been supported by Ministerio de Economía y Competitividad/FEDER, Spain [grant numbers: MTM2012-31073 and MTM2015-71200-R], Consejería de Educación Cultura y Deporte from Junta de Comunidades de Castilla-La Mancha (Spain) [grant number PEII-2014-031-P] and James S. Mc. Donnell Foundation (USA) 21st Century Science Initiative in Mathematical and Complex Systems Approaches for Brain Cancer (Special Initiative Collaborative – Planning Grant 220020420 and Collaborative award 220020450). Complex statistical methods were necessary for this paper. Víctor M. Pérez-García, Alicia Martínez-González and David Molina (Matemáticos) have significant statistical expertise. Institutional Review Board approval was obtained. Written informed consent was obtained from all subjects (patients) in this study. Methodology: retrospective, observational, multicenter study.

## References

- Stupp R, Mason WP, van den Bent MJ, Weller M, Fisher B, Taphoorn MJ et al (2005) Radiotherapy plus concomitant and adjuvant temozolomide for glioblastoma. *N Engl J Med* 352:987–996
- Ellingson BM (2015) Radiogenomics and imaging phenotypes in glioblastoma: novel observations and correlation with molecular characteristics. *Curr Neurol Neurosci Rep* 15:506
- Zinn PO, Mahmood Z, Elbanan MG, Colen RR (2015) Imaging Genomics in Gliomas. *Cancer J* 21:225–234
- Wen PY, Macdonald DR, Reardon DA, Cloughesy TF, Sorensen AG, Galanis E et al (2010) Updated response assessment criteria for high-grade gliomas: response assessment in neuro-oncology working group. *J Clin Oncol* 28:1963–1972
- Iliadis G, Selviaridis P, Kalogera-Fountzila A, Fragkoulidi A, Baltas D, Tselis N et al (2009) The importance of tumor volume in the prognosis of patients with glioblastoma: comparison of computerized volumetry and geometric models. *Strahlenther Onkol* 185:743–750
- Mazurowski MA, Zhang J, Peters KB, Hobbs H (2014) Computer-extracted MR imaging features are associated with survival in glioblastoma patients. *J Neurooncol* 120:483–488
- Zinn PO, Sathyan P, Mahajan B, Bruyere J, Hegi M, Majumder S et al (2012) A novel volume-age-KPS (VAK) glioblastoma classification identifies a prognostic cognate microRNA-gene signature. *PLoS One* 7:e41522
- Mazurowski MA, Desjardins A, Malof JM (2013) Imaging descriptors improve the predictive power of survival models for glioblastoma patients. *Neuro Oncol* 15:1389–1394
- Zacharakis EI, Morita N, Bhatt P, O'Rourke DM, Melhem ER, Davatzikos C (2012) Survival analysis of patients with high-grade gliomas based on data mining of imaging variables. *AJNR Am J Neuroradiol* 33:1065–1071
- Pérez-García VM, Calvo GF, Belmonte-Beitia J, Diego D, Pérez-Romasanta LA (2011) Bright solitary waves in malignant gliomas. *Phys Rev E* 84:021921
- Ellingson BM, Bendszus M, Boxerman J et al (2015) Consensus recommendations for a standardized Brain Tumor Imaging Protocol in clinical trials. *Neuro Oncol* 17:1188–1198
- Goel MK, Khanna P, Kishore J (2010) Understanding survival analysis: Kaplan-Meier estimate. *Int J Ayurveda Res* 1:274–278
- Zhang Z, Jiang H, Chen X, Bai J, Cui Y, Ren X et al (2014) Identifying the survival subtypes of glioblastoma by quantitative volumetric analysis of MRI. *J Neurooncol* 119:207–214
- Ramakrishna R, Barber J, Kennedy G, Rizvi Win RH, Ojemann GA, Berger MS et al (2010) Imaging features of invasion and pre-operative and postoperative tumor burden in previously untreated glioblastomas: correlation with survival. *Surg Neurol Int* 1:40
- Gutman DA, Cooper LA, Hwang SN et al (2013) MR imaging predictors of molecular profile and survival: multi-institutional study of the TCGA glioblastoma data set. *Radiology* 267:560–569
- Wangaryattawanich P, Hatami R, Wang J et al (2015) Multicenter imaging outcomes study of The Cancer Genome Atlas glioblastoma patient cohort: imaging predictors of overall and progression-free survival. *Neuro Oncol* 17:1525–1537
- Deisboeck DS, Guiot C, Delsanto PP, Pugno N (2006) Does cancer growth depend on surface extension? *Med Hypotheses* 67:1338–1341
- Macyszyn L, Akbari H, Pisapia JM, Da X, Attiah M, Pigrish V, et al (2015) Imaging patterns predict patient survival and molecular subtype in glioblastoma via machine learning techniques. *Neuro Oncol* 18:417–425
- Itakura H, Achrol AS, Mitchell LA, Loya JJ, Liu T, Westbroek EM et al (2015) Magnetic resonance image features identify glioblastoma phenotypic subtypes with distinct molecular pathway activities. *Sci Transl Med* 7:303ra138